Application of Surface Mapping to Visualize Wall Shear Stress and Particles deposition in a Realistic Human Nasal Cavity

***Yidan Shang, Kiao Inthavong, and Jiyuan Tu**

School of Aerospace, Mechanical & Manufacturing Engineering, RMIT University, Australia.
*Corresponding author: s3395646@student.rmit.edu.au

Abstract

Nasal cavity is an important component of respiration system for the various physiological functions (Elad et al., 2008; Lee, 2010). By using a commercial CFD software Ansys-Fluent and a surface mapping software Unfold3D, wall shear stress (WSS) distribution and particle deposition patterns on the nasal cavity wall were simulated and transformed into a normalized UV domain (where U and V denote coordinate axes of a 2D space) to present a complete view of an entire wrapped surface, therefore to be analyzed with better precision and to allow direct comparisons between left and right cavities. In this paper, applications of surface mapping methods on a nasal cavity are demonstrated, and results for WSS distribution and time dependent particle deposition on UV domain during steady inhalation are analyzed.

Keywords: nasal cavity, UV-mapping, CFD

Introduction

The interactions between the nasal cavity surface wall, inhaled air and inhaled particles all occur simultaneously during inhalation. Intra-individual differences is found between left and right nasal chambers, and temporal variations caused by nasal cycling (Eccles, 1996). Moving air passing over the nasal cavity walls creates a wall shear stress (WSS) (Elad et al., 2006). Recent WSS mapping on surface walls in hemodynamic studies have helped establish risk assessments of aneursyms (Goubergrits et al., 2012; Reneman et al., 2006). Displaying the WSS contour over the 3D domain allows a qualitative result that can reveal local concentrated stresses. However the representation of 3D model results is limited to digital media and typically software to view and rotate the model. Doorly (2008) analysed the effect of flow instability on WSS, by mapping out the WSS occurring along the perimeter of one cross-sectional slice. Using this method it would be ineffective to display all possible WSS profiles along the perimeter of cross-section slices to map out the entire cavity wall.

An alternative is to transform the 3D model into a 2D domain by the UV-mapping method widely used in the computer graphics industry. The letters U and V denote the coordinate axes of the 2D domain while X, Y, Z are retained in the 3D coordinate axes. This is highly effective for reporting results of nasal cavities in 2D format since both septal and lateral wall surfaces can be displayed simultaneously. The 3D model is then transformed into a 2D space representation by 'unwrapping' the model along a cut edge and the WSS data is then mapped along the entire surface wall of the 2D domain, to highlight localized regions. Furthermore, transient particles can also be mapped onto a UV domain to highlight localized concentration regions.

Method

Model description

The CFD model of human nasal cavity obtained through CT scans from a healthy 25-year old, Asia male (170 cm height, 75 kg mass) (Inthavong et al. 2011) has been created. Grid independence was

tested and the mesh was refined in the near wall and regions of high curvature. The computational model was divided into eight sections, by seven slices and labelled as S1 to S7 (Figure 1). Cross sectional slices showing the internal mesh is taken at S2, S4, and S6 which lay approximately in the nasal valve, turbinate near posterior choanae region. Two straight extension pipes, one at the inlet, and one at the outlet were created into the geometry to satisfy a fully developed flow assumption. Since the cross-sectional area decreases sharply behind the nasal pharynx, a transition section was created from the original model to connect nasal cavity with the extension of outlet.

The inlet extension has a pressure boundary condition set to zero gauge pressure to mimic the ambient surrounding environment. To simulate flow patterns of different flow rates, the extension of outlet was set as velocity outlet with the required negative velocity. A laminar flow field was adopted for the flow rates 10 L/min

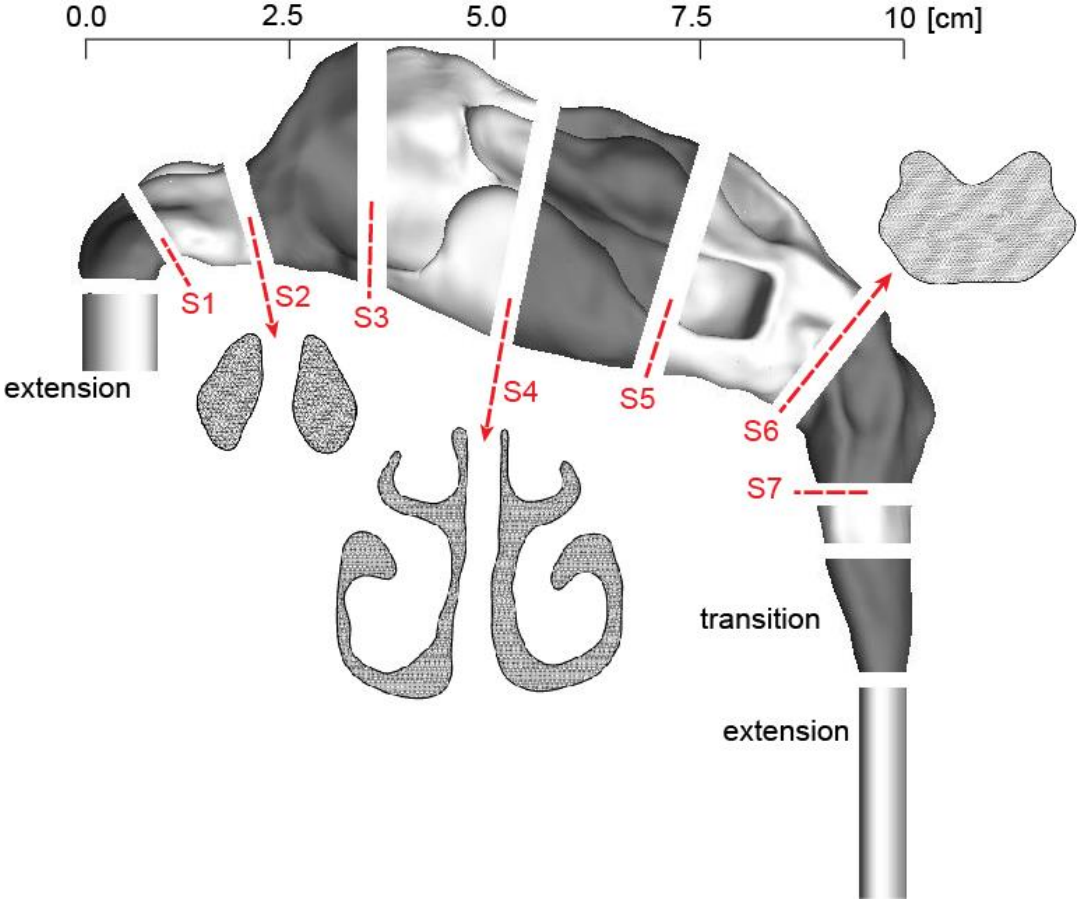

Figure 1. Nasal cavity geometry with sectioned slices,labelled S1 to S7.

UV-Mapping

Figure 2 shows Matlab connecting CFD software Ansys-Fluent and UV-Mapping software Unfold 3D to convert a 3D model to a 2D domain. The data containing information regarding the 3D nasal cavity geometry from Ansys-Fluent is outputted and accessed through Matlab. The data is rearranged so that it conforms to the .obj file format which can be imported into Unfold 3D. Within the software, the 3D model is unwrapped at a defined seam based on the ISOMAP algorithm (Tenenbaum et al., 2000). The converted 2D geometry with new coordinates in the UV domain is exported back into Matlab and is coupled with solution data obtained from CFD in the form of the flow variables WSS and particles location.

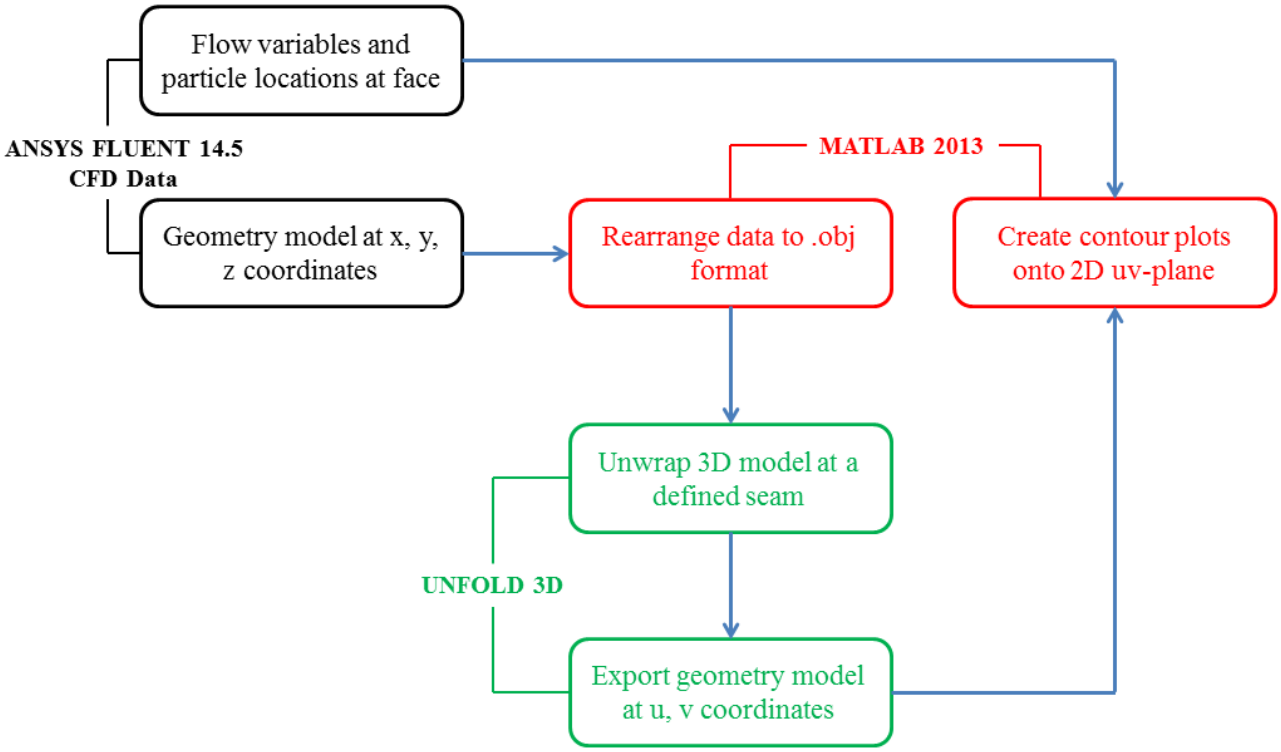

Figure 2. Flow chart showing the transformation from a cavity geometry in 3D domain into a 2D domain.

Graphically Figure 3 presents the flow process. Firstly the nasal cavity is divided into the left and right chambers. Each chamber is then unwrapped by creating a cutting slice along the bottom of the geometry to create a common reference boundary in which the surface coordinates can be related to. This common boundary edge is separated by the inlet and outlet of the nasal chamber. Furthermore the selection of the nasal floor ensures correct topology in the UV domain for regions of overlapping geometry such as that found in the meatus airway.

A further mapping normalizes the UV domain into a dimensionless rectangular space to provide better visualization. Direct comparisons between individual nasal cavity geometries can be made in normalized 2D form. This will provide a means for determining persistent flow features among all different geometries during nasal cavity inhalation. Finally projection of characteristic lines, serving as visual markers, are created based on the slices S1 to S7 (see Figure 1) and the ceiling of the inferior meatus, middle meatus and the medial nasal septum.

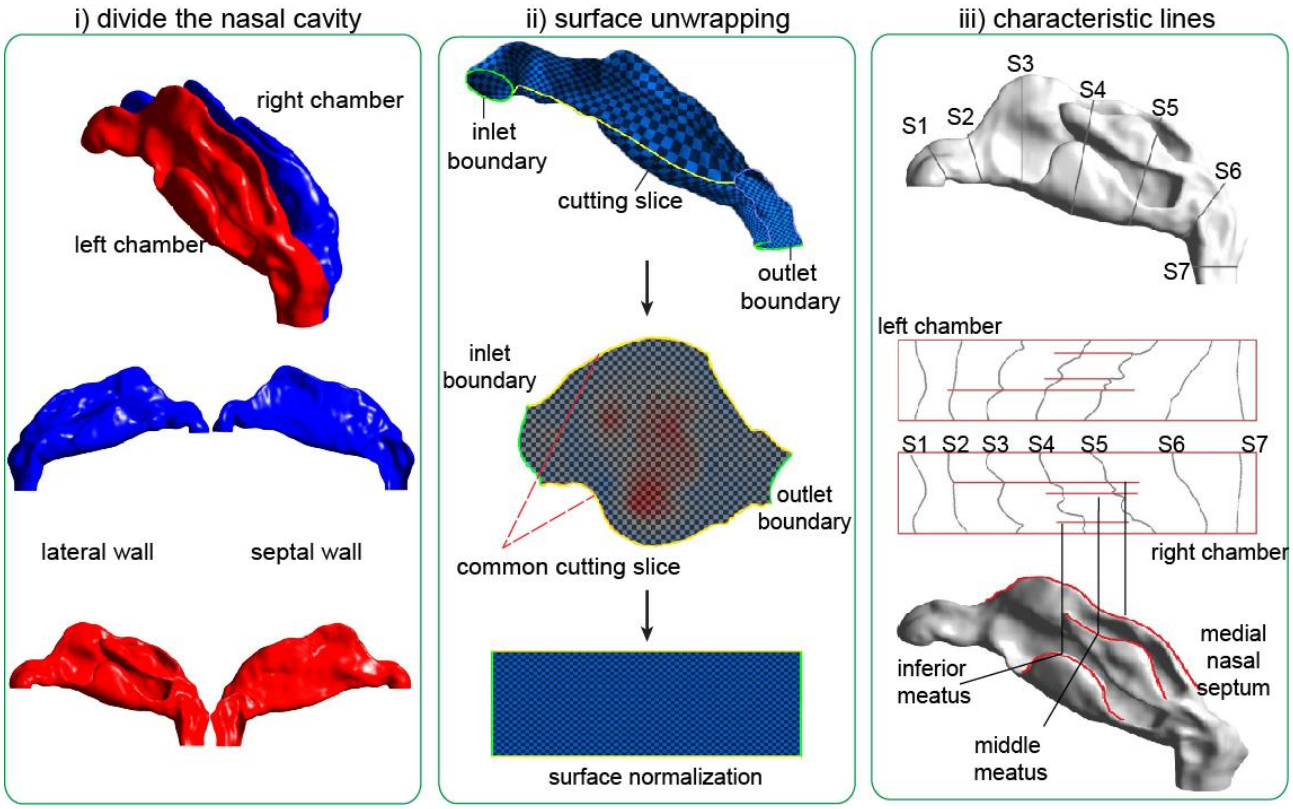

Figure 3. Flow process in unwrapping the surface of a 3D model into a 2D domain. Characteristic lines are defined at the apex of the septum wall, middle meatus, and inferior meatus.

Results

WSS Distribution Mapping

In 3D domain the nasal cavity can be displayed from one perspective view only. Figure 4 demonstrates the advantages of UV-Mapping. Under a flow rate of 10L/min, the high WSS region A and region B on both lateral and septal slides, which are hidden at the bottom of the nasal model in the 3D view, are clearly displayed in the UV domain. This suggests the inhaled air disperses laterally and shears across the side walls of each chamber as it enters the nasal vestibule. Local peaks C of approximately 0.3Pa are found in the region between the middle meatus and lateral wall in both chambers. As shear stresses are linearly related to the local velocity, these values significantly increase as breathing efforts increase. High shear stresses that are concentrated locally may also cause irritation of the blood vessels within that area.

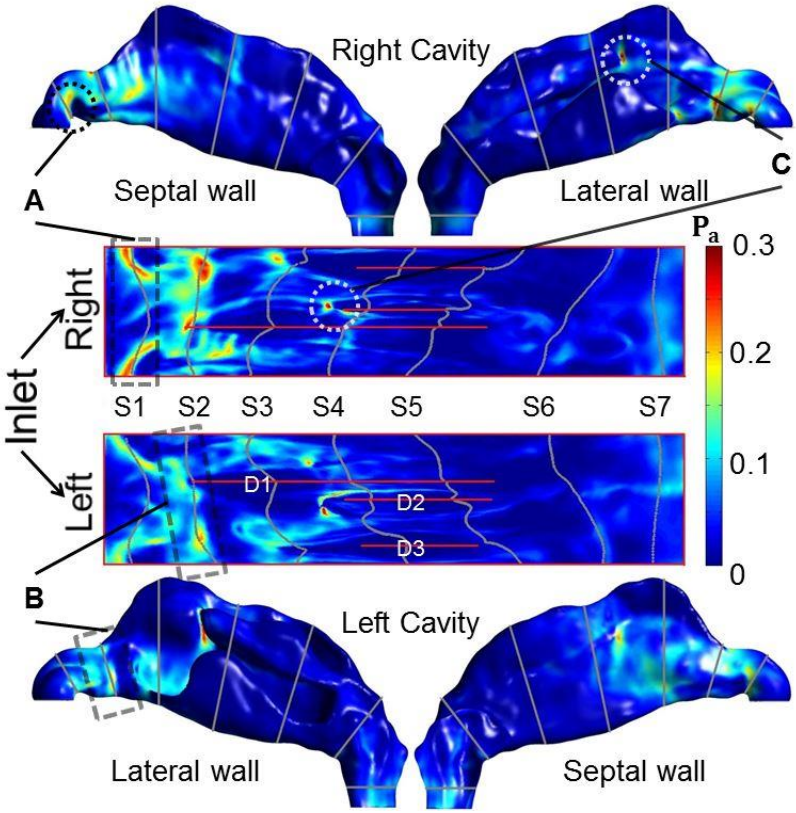

Figure 4. Local peaks, identified with the red arrows, are found near slice S4. The three red lines running in the axial direction are the characteristic lines defined in Figure 3.

10μm Particle Deposition

The total deposition efficiency of 10μm particles is shown in Figure 5 where there is higher deposition in the left chamber (21.9% deposition) and lower value in the right chamber (18.8% deposition) which is attributed to the different flow patterns caused by the differences in geometry. The greater resistance in the left airway shown in Figure 5(c) suggests a more intricate and narrow passageway that enhances the particle deposition.

Figure 6 shows the different deposition fractions (25%, 50%, 75%, and 100%) of all deposited particles patterns and its corresponding residence time in the UV domain. Deposition in preferential local regions are established early where 25% of deposited particles occur within t = 0.036 seconds and this pattern continues for up to 75% of the deposited particles by t = 0.093 seconds. The remaining 25% of particles take longer to settle, up to t = 2.045s. This may be caused by the particles being caught in recirculating regions shown in Figure 5(d)(e) and therefore producing a scatter pattern. Interestingly an unsteady inhalation cycle takes approximately 2s before exhalation occurs, and therefore it is expected that nearly all deposited particles have sufficient time to impact onto the airway surface before exhalation occurs, given that there will be decelerated flow during the end of the inhalation cycle.

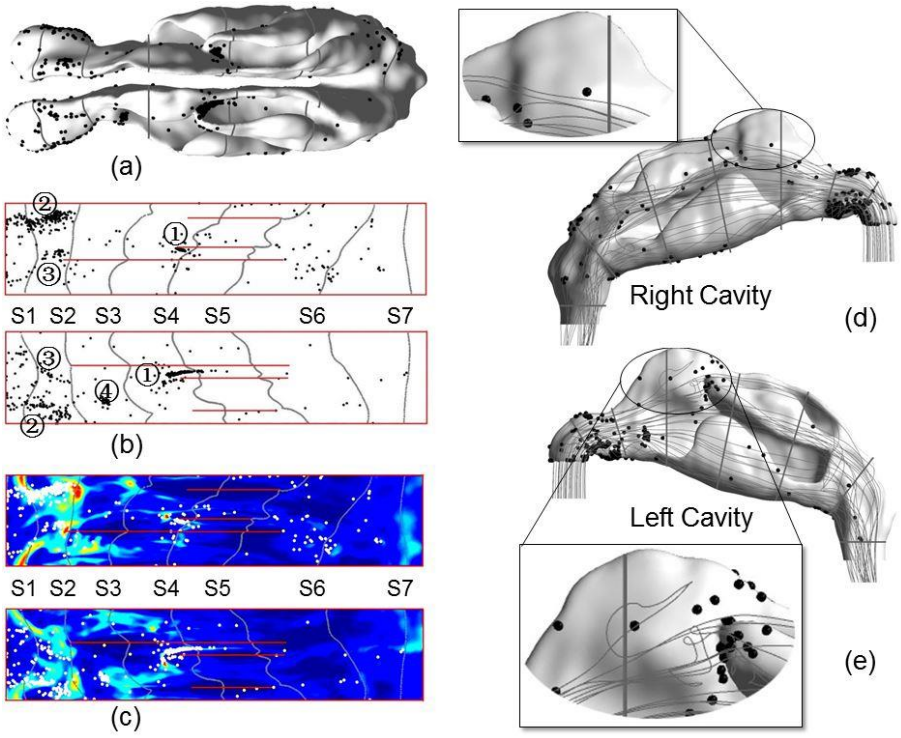

Figure 5. Nasal deposition patterns for 10μm particles in 3D and UV domains. (a). Top view of 3D particles deposition pattern. (b). Particles deposition pattern in UV domain. (c). Deposition pattern with background of WSS. (d)(e). Deposition patterns with flow streamlines showing the influence from the inhaled air.

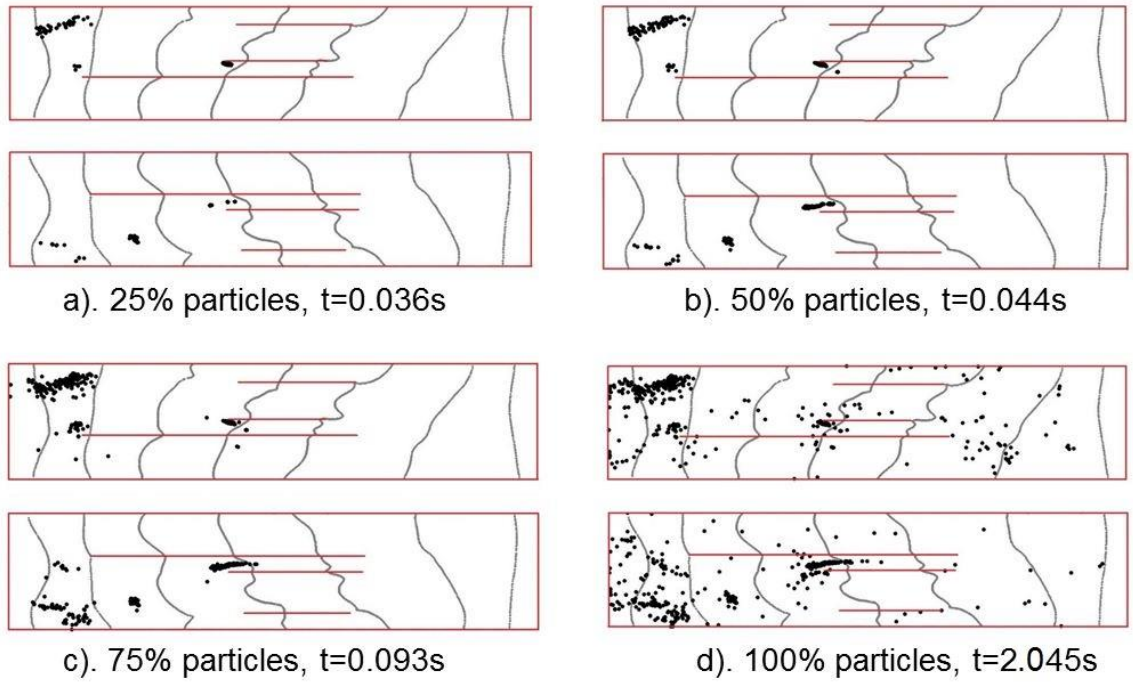

Figure 6. Time dependent deposition patterns for 10μm particles in the UV domain. Each image represents the total fraction of all deposited particles.

Conclusions

UV-Mapping method, which transforms the nasal cavity wall in 3D domain into 2D domain, provides a deeper insight into the physiological mechanisms involved with respiratory airflow. The pressure distribution was mapped onto the UV domain which showed a higher resistance in the anterior regions of the left nasal chamber, suggesting that the geometry is susceptible to impediment to flow. This may be in the form of a more narrowed geometry, high curvatures or regions leading to flow separation. Wall shear stresses, which lead to mechano-physical responses in the epithelium surfaces, are mapped which revealed the most vulnerable regions in the form of peaks occurring in the anterior nasal chambers and at the entrance of the middle meatus passageway. This mapping technique allows precise predictions of local regions that are disposed to high shearing which is not possible in 3D mode. The visualization technique presented can be used to make direct comparisons between left and right nasal chambers by normalizing UV mapped geometries. The predictions of particle deposition provided insight into likely deposition regions which were in the anterior nasal regions and middle meatus. These regions corresponded with the local WSS peaks and high resistance regions, however there needs further studies to quantify this correlation. Time dependent particle deposition was also mapped which showed that most of the particle deposition occurred within the 1.0secs of residence time in the nasal cavity In this study, a visualization technique is presented that takes a 3D wrapped surface and maps it onto a UV domain, which extends the current CFD technology and capability in visualizing the fluid flow dynamics.

References

Elad, D., Wolf, M., Keck, T., 2008. Air-conditioning in the human nasal cavity. Respiratory Physiology & Neurobiology 163, 121-127.

Lee, J.-H., Na, Y., Kim, S.-K., Chung, S.-K., 2010. Unsteady flow characteristics through a human nasal airway. Respiratory Physiology & Neurobiology 172.

Eccles, R., 1996. A role for the nasal cycle in respiratory defence. Eur Respir J 9, 371-376.

Elad, D., Naftali, S., Rosenfeld, M., Wolf, M., 2006. Physical stresses at the air-wall interface of the human nasal cavity during breathing. Journal of Applied Physiology 100, 1003-1010.

Goubergrits, L., Schaller, J., Kertzscher, U., van den Bruck, N., Poethkow, K., Petz, C., Hege, H.C., Spuler, A., 2012. Statistical wall shear stress maps of ruptured and unruptured middle cerebral artery aneurysms. J R Soc Interface 9, 677-688.

Reneman, R.S., Arts, T., Hoeks, A.P., 2006. Wall shear stress--an important determinant of endothelial cell function and structure--in the arterial system in vivo. Discrepancies with theory. J Vasc Res 43, 251-269.

Doorly, D.J., Taylor, D.J., Schroter, R.C., 2008. Mechanics of airflow in the human nasal airways. Respiratory Physiology & Neurobiology 163, 100-110.

Inthavong, K., Ge, Q., Se, C.M.K., Yang, W., Tu, J.Y., 2011. Simulation of sprayed particle deposition in a human nasal cavity including a nasal spray device. Journal of Aerosol Science 42, 100-113.

Tenenbaum, J.B., Silva, V.d., Langford, J.C., 2000. A Global Geometric Framework for Nonlinear Dimensionality Reduction. Science 290, 2319-2323.